13th International Symposium on Turbulence and Shear Flow Phenomena (TSFP13)
Montreal, Canada, June 25–28, 2024

QUANTIFYING MIXING IN FLOWS TRANSPORTING MULTIPLE SCALARS

Alaïs Hewes
Department of Mechanical Engineering
McGill University
Montréal, QC, Canada
alais.hewes@mail.mcgill.ca

Laurent Mydlarski
Department of Mechanical Engineering
McGill University
Montréal, QC, Canada
laurent.mydlarski@mcgill.ca

ABSTRACT

The present work investigates mixing metrics used to quantify multi-scalar mixing in turbulent flows. Existing multi-scalar mixing metrics, such as the scalar cross-correlation coefficient or the segregation parameter, are shown to be only capable of quantifying mixing between two scalars of interest, and fail to capture the interactions between these scalars and the surroundings in which they mix. To overcome such limitations, new multi-scalar mixing metrics (η, ξ) are proposed and then evaluated in coaxial jets transporting multiple scalars.

INTRODUCTION

A large number of scientific and engineering processes — including meteorology, climate science, environmental pollution dispersion, heat transfer, and combustion — rely upon the mixing of scalars (e.g., temperature, humidity, chemical species concentration) within turbulent flows. To predict and/or control these phenomena, we must first be able to quantify the mixing of the scalars that underlie them.

Defining Mixing

It is important to clarify what we mean by "mixing". Following the approach of Villermaux (2019), we define "mixing" to be the process by which initially segregated components evolve towards a state of homogeneity at all scales of the flow. This requires diffusion, and should be considered distinct from the process of "stirring," which, on its own, only alters the spatial organization of the concentration field.

To illustrate these differences, consider a closed system in which a black scalar of concentration $\phi = 1$ and white fluid of concentration $\phi = 0$ are initially segregated as depicted in figure 1(a). Now, assume this system is stirred: in the absence of diffusion, there is no mixing, and the black scalar remains segregated from the white fluid at scales greater than or equal to the smallest ones of the flow. As may be observed in figure 1(b), the spatial organization of the concentration field has been altered, such that the system appears well-blended. However, the composition of the concentration field remains unchanged and the probability density function for the concentration ($p(\phi)$) of the system in figure 1(b) is equal that of the system in figure 1(a):

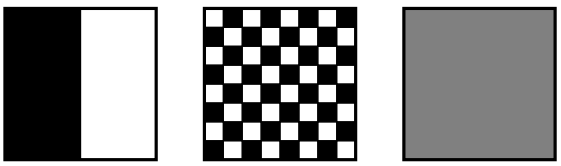

(a) (b) (c)

Figure 1: 3 possible mixing states and for a black scalar with diffusivity $\mathcal{D}$ and white fluid within a closed system: (a) initial condition of the system, (b) $\mathcal{D} = 0$, system stirred, (c) $\mathcal{D} > 0$.

$$p(\phi) = (1 - \langle\phi\rangle)\delta(\phi) + \langle\phi\rangle\delta(\phi - 1). \tag{1}$$

(Note that $\langle\phi\rangle$ denotes the mean concentration of the system and $\delta()$ is the Dirac delta function.) If, however, the diffusivity of the scalar ($\mathcal{D}$) is greater than than 0, then, regardless of whether the system is stirred or not, it will ultimately proceed to the fully mixed state illustrated in figure 1(c), where:

$$p(\phi) = \delta(\phi - \langle\phi\rangle). \tag{2}$$

Quantifying mixing requires that we be able to differentiate the mixing states depicted in figures 1(a) and (b) from that in figure 1(c), as well as any other mixing state in between.

Mixing of a single scalar with its surroundings

When a single scalar mixes with its surroundings, the scalar variance ($\langle\phi'^2\rangle$, where $\phi' \equiv \phi - \langle\phi\rangle$ represents the scalar fluctuation) is a good measure of this mixing, albeit not non-dimensional. If the scalar is perfectly unmixed with its surroundings (e.g., the systems depicted in figures 1(a) and (b)), then the scalar variance is maximized. Using equation (1), it can be shown that this maximum value is:

$$\langle\phi'^2\rangle = \langle\phi\rangle(1 - \langle\phi\rangle). \tag{3}$$

As the scalar is mixed with its surroundings, the scalar variance is gradually reduced, and, in the limit of perfect of mixing:

$$\langle \phi'^2 \rangle = 0. \tag{4}$$

Using these two extremes, a non-dimensional parameter called the unmixedness can be defined to quantify the mixing of a single scalar in ambient fluid (Danckwerts, 1952; Dimotakis & Miller, 1990):

$$\Xi = \frac{\langle \phi'^2 \rangle}{\langle \phi \rangle (1 - \langle \phi \rangle)}, 0 \leq \Xi \leq 1, \tag{5}$$

Although various other mixing metrics have been developed (e.g., the mixed-norm; Mathew *et al.*, 2005), the unmixedness parameter has the advantage of being simple — it only requires knowledge of the scalar variance and mean.

Mixing of multiple scalars with their surroundings

If the scalar variance (and its non-dimensional forms) can be used to quantify the mixing of a single scalar, then it is not unreasonable to assume that the scalar covariance ($\langle \phi_1' \phi_2' \rangle$) should quantify the mixing of multiple scalars (i.e., ϕ_1 and ϕ_2). In previous studies involving multi-scalar mixing, mixing was typically characterized using the scalar cross-correlation coefficient (ρ_{12}):

$$\rho_{12} = \frac{\langle \phi_1' \phi_2' \rangle}{\langle \phi_1'^2 \rangle^{1/2} \langle \phi_2'^2 \rangle^{1/2}}, -1 \leq \rho_{12} \leq 1, \tag{6}$$

which normalizes the scalar covariance with scalar variances (Warhaft, 1981, 1984; Sirivat & Warhaft, 1982; Tong & Warhaft, 1995; Vrieling & Nieuwstadt, 2003; Costa-Patry & Mydlarski, 2008; Cai *et al.*, 2011; Soltys & Crimaldi, 2015; Oskouie *et al.*, 2015, 2017, 2018; Li *et al.*, 2017). Many of these studies focused on the mixing of two laterally-separated scalar sources within an environment that can be approximated as infinitely large. The authors of these studies found that the scalar cross-correlation coefficient generally evolves as follows: (i) initially the correlation coefficient is undefined, as the measurement probe is rarely exposed to either of the scalar fields produced by the scalar sources, (ii) farther downstream, the measurement probe begins to alternatively sample each scalar field, but not both at the same time, so that the correlation coefficient becomes increasingly negative, and finally, (iii) the scalar plumes begin to overlap and mix, and the correlation coefficient starts to increase, eventually becoming positive and (iv) tending towards an asymptotic value of 1 when the scalars are perfectly mixed with each other (Warhaft, 1984; Tong & Warhaft, 1995; Vrieling & Nieuwstadt, 2003; Costa-Patry & Mydlarski, 2008; Oskouie *et al.*, 2015, 2017, 2018). In the aforementioned flows, the correlation coefficient can provide an adequate measure of mixing, as it can be used to identify when the scalars become perfectly mixed with each other. However, the information it provides is limited, and occasionally ambiguous; negative values of the correlation coefficient may indicate both a state in which the scalars remain segregated and one in which the scalars have begun to overlap and mix. More importantly, after analyzing the asymptotic behavior of the correlation coefficient for several key mixing states, we find that it is not a suitable mixing metric in all flows. Values of the correlation coefficient at these key mixing states are listed in table 1, where it can be observed that ρ_{12} will become undefined in a closed system in which ϕ_1, ϕ_2, and their surroundings are perfectly mixed.

One common alternative to the scalar cross-correlation coefficient is the segregation parameter (α_{12}):

$$\alpha_{12} = \frac{\langle \phi_1' \phi_2' \rangle}{\langle \phi_1 \rangle \langle \phi_2 \rangle}, \alpha_{12} \geq -1, \tag{7}$$

which normalizes the scalar covariance by scalar means, and is often used in the context of reactive flows (e.g., Komori *et al.*, 1991). This mixing metric is derived in the same manner as the unmixedness parameter given in equation (5) — by solving for the value of the covariance in the limit of no mixing between the scalars and their surroundings and then normalizing the covariance using this value. As shown in table 1, α_{12} has the advantage of being clearly defined when the scalars have yet to mix with each other ($\alpha_{12} = -1$) and in the limit of perfect mixing between both scalars and their surroundings ($\alpha_{12} = 0$), making it a generally more effective mixing metric than ρ_{12}. Nevertheless, the segregation parameter has a significant shortcoming — as shown in table 1, a single value α_{12} may refer to different mixing states.

Ultimately, the problem with using ρ_{12}, α_{12}, or any other form of the covariance to quantify multi-scalar mixing is that these mixing metrics only offer insight into how the two scalars of interest (ϕ_1, ϕ_2) are mixed with each other, and not not how they are mixed with their environment. Our objective herein is to develop new mixing metrics which can measure both how scalars mix with each other *and* how they mix with their surroundings. Then we will assess their effectiveness in real flows transporting multiple scalars.

DEVELOPMENT OF NEW MULTI-SCALAR MIXING METRICS

To better understand multi-scalar mixing one can treat the surrounding fluid as an additional scalar. This convention has previously been used in a number of studies, including Cai *et al.* (2011), and Li *et al.* (2017), which is why the mixing of two scalars with their surroundings may sometimes also be referred to as 3-scalar mixing. Using this perspective, we consider the mixing of two scalars, ϕ_1 and ϕ_2, in ambient fluid represented by ϕ_3. We can define an unmixedness tensor (Ξ_{ij}) which accounts for the unmixedness of each possible scalar combination within this flow:

$$\Xi_{ij} = \begin{bmatrix} 0 & \alpha_{12} & \alpha_{13} \\ \alpha_{12} & 0 & \alpha_{23} \\ \alpha_{13} & \alpha_{23} & 0 \end{bmatrix}. \tag{8}$$

The unmixedness of two different scalars (e.g., ϕ_1 and ϕ_2) is characterized by the segregation parameter of these two scalars (e.g., α_{12}), because, as discussed in the previous section, it is a more effective mixing metric than the correlation coefficient. We define the unmixedness between a scalar and itself, which is represented by the components along the diagonal of Ξ_{ij}, to be equal to 0 because a scalar will always be perfectly mixed with itself.

A few points must be made about Ξ_{ij}. First, since $\alpha_{12} = \alpha_{21}$, Ξ_{ij} is symmetric, and represented as such. Second, despite having only segregation parameters as its non-zero components, we refer to Ξ_{ij} as the unmixedness tensor because

Table 1: Values of ρ_{12} and α_{12} for several key mixing states

Mixing State	ρ_{12}	α_{12}
ϕ_1, ϕ_2, & surroundings not mixed	$-\left[\frac{\langle\phi_1\rangle\langle\phi_2\rangle}{(1-\langle\phi_1\rangle)(1-\langle\phi_2\rangle)}\right]^{1/2}$	-1
ϕ_1 & surroundings perfectly mixed, ϕ_2 & surroundings not mixed	-1	-1
ϕ_1 & ϕ_2 perfectly mixed, but not mixed with surroundings	1	$\frac{1-\langle\phi_1\rangle-\langle\phi_2\rangle}{\langle\phi_1\rangle+\langle\phi_2\rangle}$
ϕ_1, ϕ_2 & surroundings perfectly mixed	Undefined	0

the term unmixedness is a better and more accurate descriptor[1]. Third, it should be noted that the third scalar in the flow is not actually independent from the other two, since $\phi_1 + \phi_2 + \phi_3 = 1$. Accordingly, its statistics may be expressed in terms of those of ϕ_1 and ϕ_2:

$$\langle\phi_1'\phi_3'\rangle = -\langle\phi_1'^2\rangle - \langle\phi_1'\phi_2'\rangle, \tag{9a}$$

$$\langle\phi_2'\phi_3'\rangle = -\langle\phi_2'^2\rangle - \langle\phi_1'\phi_2'\rangle, \tag{9b}$$

$$\langle\phi_3'^2\rangle = \langle\phi_1'^2\rangle + \langle\phi_2'^2\rangle + 2\langle\phi_1'\phi_2'\rangle. \tag{9c}$$

However α_{12}, α_{13}, and α_{23} *are* independent from each other. This is because the segregation parameter is a normalized covariance. Moreover, although only 3 of the 6 variances and covariances appearing in equations (9a), (9b), (9c) are actually independent, which 3 to take as independent is an arbitrary choice. $\langle\phi_1'^2\rangle$, $\langle\phi_2'^2\rangle$, and $\langle\phi_3'^2\rangle$ can all be expressed as functions of the 3 covariances, such that $\langle\phi_1'\phi_2'\rangle$, $\langle\phi_1'\phi_3'\rangle$, and $\langle\phi_2'\phi_3'\rangle$ can be considered independent from each other and used to fully describe the flow.

To further simplify Ξ_{ij}, we calculate the invariants of this tensor:

$$\mathrm{I} = 0, \tag{10a}$$

$$\mathrm{II} = -(\alpha_{12}^2 + \alpha_{13}^2 + \alpha_{23}^2), \tag{10b}$$

$$\mathrm{III} = 2\alpha_{12}\alpha_{13}\alpha_{23}. \tag{10c}$$

As shown above, Ξ_{ij} has two independent invariants, from which we can define two new mixing metrics, η and ξ:

$$\eta^2 = -\frac{1}{3}\mathrm{I} = \frac{1}{3}(\alpha_{12}^2 + \alpha_{13}^2 + \alpha_{23}^2), \tag{11}$$

$$\xi^3 = \frac{1}{2}\mathrm{II} = \alpha_{12}\alpha_{13}\alpha_{23}. \tag{12}$$

The use of η and ξ allows us to characterize Ξ_{ij}, with 2 rather than 3 components, making it easier to graphically represent the state of mixing within the flow.

EXPERIMENTAL INVESTIGATION

In the second part of this paper we examine the mixing of two scalars — helium concentration and temperature — within turbulent coaxial jets to better understand the limitations of current multi-scalar mixing metrics (i.e., the scalar-cross correlation coefficient and segregation parameter) and assess the effectiveness of the novel mixing metrics (η and ξ) developed in the previous section.

[1] In fact, α_{12} could also be referred to as an unmixedness parameter, since in 2-scalar mixing ($\phi_3 = 0$) $\alpha_{12} = -\Xi$.

Apparatus and Instrumentation

As illustrated in figure 1, the coaxial jets consist of: (i) a center jet containing an (unheated) mixture of helium and air, (ii) an annular jet containing pure (unheated) air, and (iii) a coflow containing (pure) heated air. A 3-wire thermal anemometry-based probe composed of an interference probe and cold-wire thermometer was secured to a 3-axis traversing mechanism to measure helium concentration and temperature at select locations within the flow. The interference probe consists of two hot-wires placed close enough together that one is in the thermal field of the other, and is used to measure velocity and gas concentration in turbulent flows. It is placed within 1 mm of a cold-wire thermometer sensor, which measures temperature independently of velocity and helium concentration (Hewes & Mydlarski, 2021*a*,*b*). The 3-wire probe was operated using a TSI IFA300 constant temperature anemometer and custom-made constant current anemometer. Signals from each of the wires were filtered with Krohn-Hite 3382 and 3384 filters, and then digitized with a 16-bit National Instrument PCI-6143 data acquisition board. The measured helium concentrations and temperatures were normalized to be equal to 1 at their respective jet exits. Accordingly, the unheated pure air from the annular jet (ϕ_2) could be inferred from:

$$\phi_2 = 1 - \phi_1 - \phi_3, \tag{13}$$

where ϕ_1 is the normalized helium concentration and ϕ_3 is the normalized temperature (Hewes & Mydlarski, 2023). For any additional information on the apparatus, instrumentation, and post-processing of the data see Hewes & Mydlarski (2023).

Experiments

Measurements were performed along the axis of the coaxial jets for the three momentum flux ratios (M) listed in table 2. In each case, the momentum flux (and Reynolds number) of the center jet was held constant. The center jet was supplied with a mixture composed of 6% helium and 94% air by mass ($C_1 = 0.06$), and the coflow was heated such that there was a 7.0°C difference in temperature between the coflow and center jet ($\Delta T_{max} = T_3 - T_1 = 7.0$°C, where T_1 and T_3 are the temperatures at the exits of the center jet and coflow, respectively). The combined buoyancy effects of these scalars was found to be negligible, as the ratio of production of turbulent kinetic energy by buoyancy to the dissipation rate of turbulent energy (i.e., $\frac{g\langle u\rho\rangle}{\langle\rho\rangle}/\varepsilon$) was estimated to be at most 0.03% for all cases. Thus, the scalars measured in this work were deemed passive.

Results

Measurements of the correlation coefficients ρ_{12}, ρ_{13}, and ρ_{23} are presented in figure 3. Initially, $\rho_{12} \approx -1$, indicating

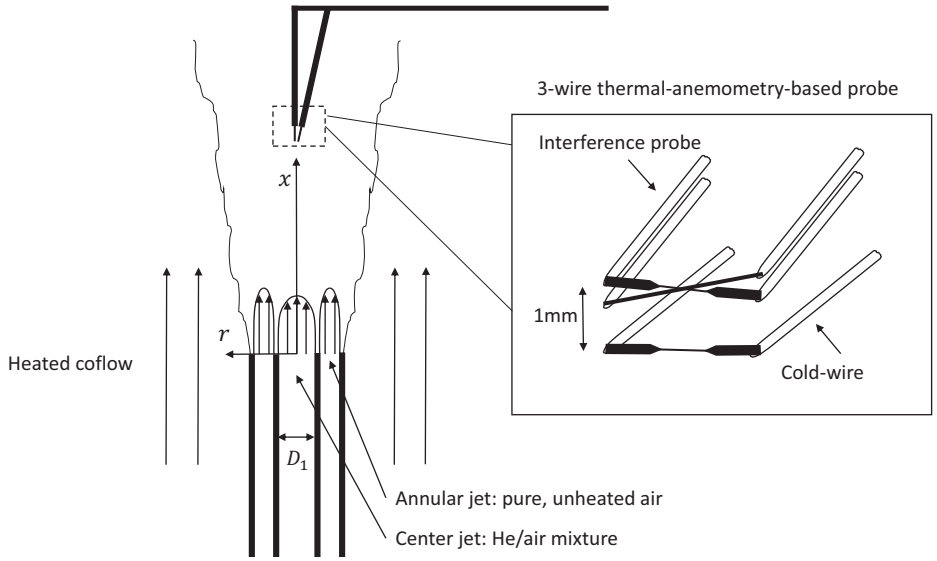

Figure 2: Schematic of the coaxial jet apparatus and 3-wire thermal-anemometry-based probe. Figure reproduced from Hewes & Mydlarski (2023).

Table 2: Properties of the flow in the center jet, annular jet and coflow for the three cases investigated, including the momentum flux ratio ($M = M_2/M_1$, where M_1 is the momentum flux of the center jet, and M_2 is the momentum flux of the annular jet), the He mass fraction at the exit of the center jet (C_1), the temperature difference between the center jet and coflow ($\Delta T_{\max}$), the Reynolds number of the center and annular jets (respectively Re_D, Re_{D_h}), and the velocity of the coflow (U_3).

Case	C_1	$\Delta T_{\max}$ (°C)	Re_D	Re_{D_h}	U_3 (m/s)
I: $M = 0.77$	0.06	7.0	3700	2000	0.4
II: $M = 2.1$	0.06	7.0	3700	3400	0.4
III: $M = 4.2$	0.06	7.0	3700	4700	0.4

that ϕ_1 and ϕ_2 are anti-correlated. Measurement of one scalar implies absence of the other. Farther downstream, as ϕ_3 is introduced into the flow, and ϕ_1 and ϕ_2 are mixed together, ρ_{12} increases and ρ_{13} and ρ_{23} decreases. It is expected that eventually ρ_{12} will tend to 1, denoting perfect mixing of ϕ_1 and ϕ_2. Accordingly, using the relationships provided in equations (9a), (9b), and (9c), one can show that:

$$\rho_{13,x\to\infty} = \rho_{23,x\to\infty} = -1 \tag{14}$$

As can be observed in figure 3, these asymptotic conditions are not always fully reached in the range of measurements presented herein. (Reduced signal-to-noise ratio of the measurements far downstream, as well as differences in the scalar diffusivities may also explain why asymptotic conditions are not observed; Hewes & Mydlarski, 2023). Nevertheless, one can see that ρ_{12} tends to large positive values and ρ_{23} approaches -1 more quickly as M increases, which suggests that increasing this parameter could improve mixing within the flow.

As correlation coefficients give no insight into when the scalars of interest begin mixing, segregation parameters are plotted in figure 4. The results presented in this figure demonstrate that at $x/D_1 = 3.2$, $\alpha_{12} > -1$, which indicates that ϕ_1 and ϕ_2 have already begun to mix with each close to the jet exit. Moreover, ϕ_1 and ϕ_3, as well as ϕ_2 and ϕ_3, are also starting to mix by $x/D_1 = 6.4$ and are relatively well-mixed by $x/D_1 = 25.1$, since $\alpha_{13} \approx \alpha_{23} \approx 0$ at this point. None of the above can be inferred from measurements of the correlation coefficients, which is why the segregation parameter should be preferred over the correlation coefficient.

If $\rho_{12,\to\infty} = 1$ far downstream, then α_{12} should approach a small, positive, constant value:

$$\alpha_{12,x\to\infty} = \frac{1\cdot\phi_{1,rms}\phi_{2,rms}}{\langle\phi_1\rangle\langle\phi_2\rangle} = \frac{\phi_{1,rms}}{\langle\phi_1\rangle}\frac{\phi_{2,rms}}{\langle\phi_2\rangle} = \text{cst}, \tag{15}$$

where $\phi_{rms} = \langle\phi'^2\rangle^{1/2}$, and α_{13} and α_{23} should both tend towards 0:

$$\alpha_{13,x\to\infty} \propto \alpha_{23,x\to\infty} \propto \frac{\phi_{3,rms}}{\langle\phi_3\rangle} \to 0. \tag{16}$$

This behavior can be observed in figure 4. Similarly to the evolution of ρ_{12}, α_{12} increases to its asymptotic value more quickly as M is increased. However both α_{13} and α_{23} appear to tend towards zero more slowly as M increases. Similar conflicting trends in mixing were were identified in Hewes & Mydlarski (2023), where other statistics, including $\langle\phi_2\rangle$ and $\langle\phi_3\rangle$, were shown to approach their asymptotic limits more slowly as M was increased. This contradictory behavior motivated the present the study, as we wanted to better understand the impact of M on mixing within the flow.

To provide a better picture of the overall mixing within the flow, the newly developed mixing metrics ξ and η are plotted as a function of each other in figure 5. It is worth noting that these mixing metrics do not contain more information than what was provided in figures 4(a), (b), and (c). Rather, they condense the information of figures 4(a), (b), and (c) into a single plot, making it easier to understand how this information fits together. As was done for the correlation coefficients and segregation parameters, the asymptotic mixing condition for the flow is derived. By combining equations (11) and (12)

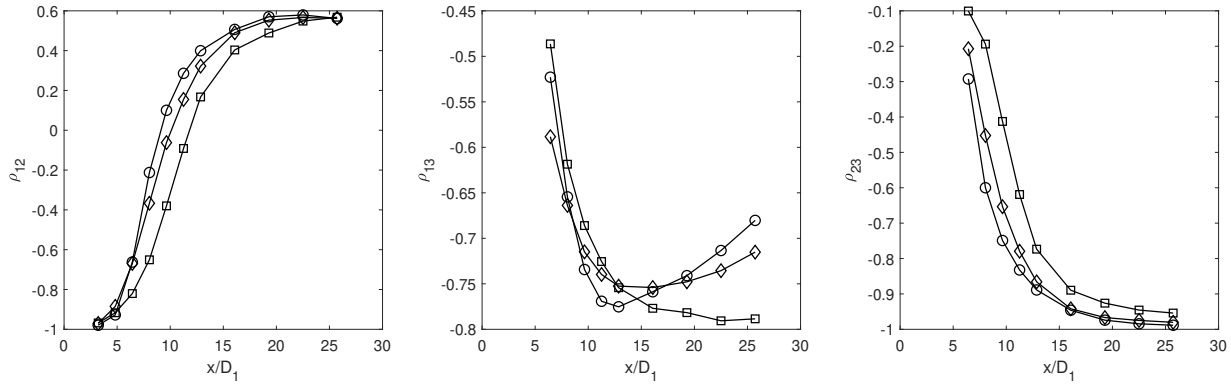

(a) (b) (c)

Figure 3: Downstream evolution of correlation coefficients along the axis of the jets for $M = 0.77$ (□), $M = 2.1$ (◇), and $M = 4.2$ (○): (a) ρ_{12}, (b) ρ_{13}, and (c) ρ_{23}. In (b) and (c), results are only plotted for $x/D_1 > 6.4$ due to limited quantities of ϕ_3 close to the jet exit. Data reproduced from Hewes & Mydlarski (2023).

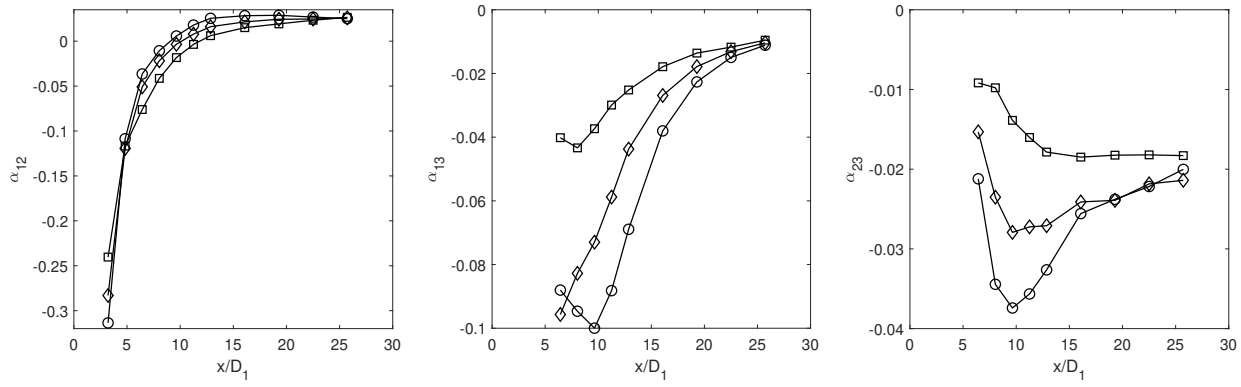

(a) (b) (c)

Figure 4: Downstream evolution of segregation parameters along the axis of the jets for $M = 0.77$ (□), $M = 2.1$ (◇), and $M = 4.2$ (○): (a) α_{12}, (b) α_{13}, and (c) α_{23}. In (b) and (c), results are only plotted for $x/D_1 > 6.4$ due to limited quantities of ϕ_3 close to the jet exit.

with equations (15) and (16), one finds that:

$$\eta = \sqrt{\frac{1}{3}\left(a^2 + \frac{1+b^2}{ab}\xi^3\right)}, \tag{17}$$

where $a = \alpha_{12,x\to\infty}$, $b = \alpha_{23,x\to\infty}/\alpha_{13,x\to\infty}$, and ξ eventually tends to 0. Although a and b are constants that can be determined from the data presented in figure 4, their true values may be masked by poor signal-to-noise ratio of the measurements far downstream. In coaxial jets, we expect that eventually $\frac{\phi_{1,rms}}{\langle\phi_1\rangle} \approx \frac{\phi_{2,rms}}{\langle\phi_2\rangle} \approx 0.2$ (Cai *et al.*, 2011). Thus, a and b can be estimated as follows:

$$a = \rho_{12,x\to\infty} \cdot 0.2^2 \approx 0.6 \cdot 0.04 \approx 0.024, \tag{18a}$$

$$b = \frac{\phi_{2,rms}}{\langle\phi_2\rangle} \Big/ \frac{\phi_{1,rms}}{\langle\phi_1\rangle} \approx 1. \tag{18b}$$

Using these estimations, equation (17) is depicted by the dashed line in figure 5. One can observe that each curve in this figure approaches and then follows the asymptotic mixing condition. Figure 5 makes clear that the flow never becomes perfectly mixed — this is only achieved when $\eta = \xi = 0$, and the asymptotic mixing condition does not tend towards this point. Furthermore, it demonstrates that the curve for $M = 0.77$ approaches the asymptotic condition fastest. Thus, the coaxial jets ultimately mix faster at lower values of M. This is in contrast to what might be concluded using only measurements of ρ_{12} or α_{12}.

CONCLUSIONS

Quantifying multi-scalar mixing is complex. When a single scalar mixes with its surroundings it, the mixedness of the system evolves along the continuum between no mixing at all and perfect mixing. But once an additional scalar is introduced into the flow, additional mixing states are also introduced. (For example, perfect mixing of one scalar with the surroundings, but no mixing between the other scalar and the surroundings; perfect mixing of both scalars with each other, but no mixing with the surroundings). Previous studies of multi-scalar mixing have relied on mixing metrics such as the scalar cross-correlation coefficient or segregation parameter which do not capture the complexity of this mixing. The segregation parameter, in particular, may be an effective mixing metric if one wishes to know how well two scalars come in contact with each other, which is useful in reactive flows, where the mixing of two reactants can determine if, and how fast, a reaction proceeds. However, the segregation parameter (like the correlation coefficient) would not adequately capture how two pollutants are mixed with their environment.

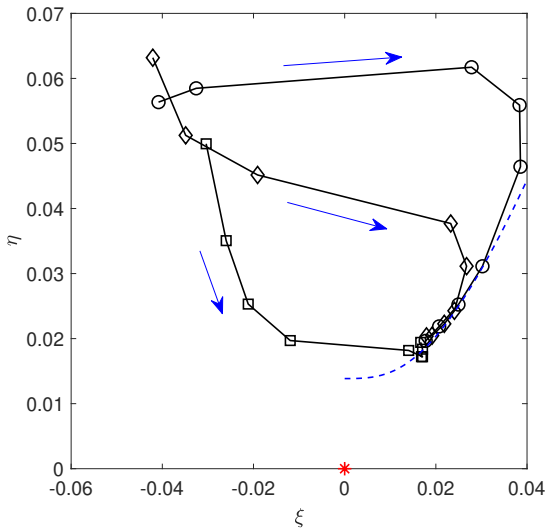

Figure 5: η plotted against ξ in the interval $6.4 \leq x/D_1 \leq 25.1$ for $M = 0.77$ (□), $M = 2.1$ (◇), and $M = 4.2$ (○). The dashed line represents the asymptotic mixing condition of the coaxial jets. Arrows indicate the direction of increasing x/D_1. The red marker indicates the values of η and ξ when the flow is perfectly mixed.

To provide a more complete description of mixing within the flow we have derived a pair of new multi-scalar mixing metrics (η and ξ) from a tensor quantifying the unmixedness between each possible scalar combination. Employing these mixing metrics within turbulent coaxial jets of different momentum flux ratios helps to better visualize the overall process of mixing within the flow, which will never become perfectly mixed, as new ϕ_3 is continuously entrained into the flow. Moreover, our new mixing metrics clarify how the momentum flux ratio affects the mixing of coaxial jets. Whether these additional insights extend to other flows transporting multiple scalars must now be explored to further validate the suitability of η and ξ as multi-scalar mixing metrics.

REFERENCES

Cai, J., Dinger, M. J., Li, W., Carter, C. D., Ryan, M. D. & Tong, C. 2011 Experimental study of three-scalar mixing in a turbulent coaxial jet. *J. Fluid Mech.* **685**, 495–531.

Costa-Patry, E. & Mydlarski, L. 2008 Mixing of two thermal fields emitted from line sources in turbulent channel flow. *J. Fluid Mech.* **609**, 349–375.

Danckwerts, P. V. 1952 The definition and measurement of some characteristics of mixtures. *App. Sci. Res., Sec. A* **3**, 279–296.

Dimotakis, P. E. & Miller, P. L. 1990 Some consequences of the boundedness of scalar fluctuations. *Phys. Fluids A-Fluid* **2** (11), 1919–1920.

Hewes, A. & Mydlarski, L. 2021*a* Design of thermal-anemometry-based probes for the simultaneous measurement of velocity and gas concentration in turbulent flows. *Meas. Sci. Technol.* **32**, 105305.

Hewes, A. & Mydlarski, L. 2021*b* Simultaneous measurements of velocity, gas concentration, and temperature by way of thermal-anemometry-based probes. *Meas. Sci. Technol.* **33** (1), 015301.

Hewes, A. & Mydlarski, L. 2023 Multi-scalar mixing in turbulent coaxial jets. *J. Fluid Mech.* **961**, A9.

Komori, S., Hunt, J. C. R, Kanzaki, T. & Murakami, Y. 1991 The effects of turbulent mixing on the correlation between two species and on concentration fluctuations in non-premixed reacting flows. *J. Fluid Mech.* **228**, 629–659.

Li, W., Yuan, M., Carter, C. D. & Tong, C. 2017 Experimental investigation of the effects of mean shear and scalar initial length scale on three-scalar mixing in turbulent coaxial jets. *J. Fluid Mech.* **817**, 183–216.

Mathew, George, Mezić, Igor & Petzold, Linda 2005 A multi-scale measure for mixing. *Physica D* **211** (1-2), 23–46.

Oskouie, S. N., Wang, B.-C. & Yee, E. 2015 Study of the interference of plumes released from two near-ground point sources in an open channel. *Intl. J. Heat Fluid Fl.* **55**, 9–25.

Oskouie, S. N., Wang, B.-C. & Yee, E. 2017 Numerical study of dual-plume interference in a turbulent boundary layer. *Bound.-Lay. Meteorol.* **164** (3), 419–447.

Oskouie, S. N., Yang, Z. & Wang, B.-C. 2018 Study of passive plume mixing due to two line source emission in isotropic turbulence. *Phys. Fluids* **30** (7), 075105.

Sirivat, A. & Warhaft, Z. 1982 The mixing of passive helium and temperature fluctuations in grid turbulence. *J. Fluid Mech.* **120**, 475.

Soltys, M. A. & Crimaldi, J. P. 2015 Joint probabilities and mixing of isolated scalars emitted from parallel jets. *J. Fluid Mech.* **769**, 130–153.

Tong, C. & Warhaft, Z. 1995 Passive scalar dispersion and mixing in a turbulent jet. *J. Fluid Mech.* **292**, 1–38.

Villermaux, E. 2019 Mixing versus stirring. *Annu. Rev. Fluid Mech.* **51**, 245–273.

Vrieling, A. & Nieuwstadt, F. 2003 Turbulent dispersion from nearby point sources – interference of the concentration statistics. *Atmos. Environ.* **37** (32), 4493–4506.

Warhaft, Z. 1981 The use of dual heat injection to infer scalar covariance decay in grid turbulence. *J. Fluid Mech.* **104**, 93–109.

Warhaft, Z. 1984 The interference of thermal fields from line sources in grid turbulence. *J. Fluid Mech.* **144**, 363.